Computationally enhanced X-ray diffraction analysis of a gold(III) complex interacting with the human telomeric DNA G-quadruplex. Unravelling non-unique ligand positioning

Damiano Cirri[a], Carla Bazzicalupi[b,*], Ulf Ryde[c,*], Justin Bergmann[c], Francesca Binacchi[a], Alessio Nocentini[d], Alessandro Pratesi[a], Paola Gratteri[d,*], Luigi Messori[b]

a Department of Chemistry and Industrial Chemistry, University of Pisa, Via G. Moruzzi 13, 56124 Pisa, Italy.

b Department of Chemistry —Ugo Schiffl, University of Florence, Via della Lastruccia 3-13, 50019 Sesto Fiorentino, Italy.

c Division of Theoretical Chemistry, Lund University, Chemical Centre, P. O. Box 124, SE-221 00 Lund, Sweden

d Department NEUROFARBA − Pharmaceutical and Nutraceutical Section and Laboratory of Molecular Modeling Cheminformatics & QSAR, University of Florence, Via U. Schiff 6, 50019 Sesto Fiorentino, Florence, Italy.

Corresponding authors: Carla Bazzicalupi (carla.bazzicalupi@unifi.it), Ulf Ryde (ulf.ryde@teokem.lu.se), Paola Gratteri (paola.gratteri@uifi.it)

Abstract

The crystal structure of the human telomeric DNA Tel24 G-quadruplex (Tel24 = TAG3(T2AG3)3T) in complex with the novel [AuL] species (with L = 2,4,6-tris(2-pyrimidyl)-1,3,5-triazine – TpymT-α) was solved by a novel joint molecular mechanical (MM)/quantum mechanical (QM) innovative approach. The quantum-refinement crystallographic method (crystallographic refinement enhanced with quantum mechanical calculation) was adapted to treat the [AuL]/G-quadruplex structure, where each gold complex in the binding site was found spread over four equally occupied positions. The four positions were first determined by docking restrained to the crystallographically determined metal ions' coordinates. Then, the quantum refinement method was used to resolve the poorly defined density around the ligands and improve the crystallographic determination, revealing that the binding preferences of this metallodrug toward Tel24 G-quadruplex arise from a combined effect of pyrimidine stacking, metal–guanine interactions and charge–charge neutralizing action of the π-acid triazine. The occurrence of interaction in solution with the Tel24 G-quadruplex DNA was further proved through DNA melting experiments, which showed a slight destabilisation of the quadruplex upon adduct formation.

Keywords

X-ray diffraction, QM/MM, DNA G-quadruplex, gold complexes, quantum refinement, melting experiments

1. Introduction

In the last decades, the guanine quadruplex (G4) non-canonical folding [1] has been recognized as an important element in the control of essential biological processes such as oncogenesis, infectious protein control, parasitic and neurodegenerative mechanisms [2]. G4s can be formed by guanine-rich DNA or RNA sequences, which arrange in square planar core motifs, called the G-tetrad or G-quartet, consisting of four guanines held by Hoogsteen hydrogen bonds. The quadruplexes are stabilized by monovalent cations such as potassium and sodium, which coordinate with the central electronegativecarbonyl O6 atoms of the G-quartet core (Figure 1 top). G4s display a wide variety of topologies, depending on the sequence, loop size, intramolecular or intermolecular strand stoichiometry, as well as strand polarity and orientation. As a rule of thumb, G-rich sequences with the potential to fold into unimolecular G4s are comprised of four consecutive G-tracts, separated by three loop regions.

Compared to the very large number of identified Putative Quadruplex Sequences (PQSs – estimated to be ~376,000 in the human genome) [3], so far only a few of them are known to have biologically relevant functions. Among them, the (TTAGGG)n telomeric sequence found at the end of eukaryotic chromosomes attract much interest, as the G-quadruplexes it can form were found to inhibit the telomerase-based cell immortalization mechanism, present in about 85% of cancer diseases [4]. These findings strongly promoted the search for small molecules able to bind or even to promote human telomeric G4s formation, as they can potentially have therapeutic and/or diagnostic applications. In this context, metal complexes [5] can represent an interesting alternative to the more explored organic ligands [6], due to the variability deriving from the efficient metal driven assembly of building blocks with potentially diverse features. In addition, the positive charge of the metal centres conveniently complements the anionic nature of the nucleic acids.

Despite the growing interest in medicinal applications of transition metal complexes, very little structural information is available in the literature concerning the binding of metal complexes to G4s. Indeed, among the numerous references published during the last ten years [7], only ten papers report structures solved in atomic detail by X-ray diffraction (Protein Data Bank (pdb) [8] codes: 3QSC, 3QSF, 5CCW, 5LS8, 6H5R, 6RNL, 6XCL) or solution NMR techniques (pdb codes: 2MCC, 2MCO, 5MVB, 5Z8F, 5Z80, 6LNZ).

Notably, most of these studies concern platinum or gold complexes, most likely because these metals are intensely studied due to their large anticancer potential (cf. cisplatin and its analogues carboplatin and oxaliplatin, which are in widespread clinical use) [9]. Gold-containing compounds attract attention also for their antimicrobial or antiparasitic activities [10]. In addition, the electronic configurations, associated with the common oxidation states of both elements, typically lead to square-planar (d^8 – Pt^{2+} and Au^{3+}) or linear geometries (d^{10} – Au^{+}), which favour DNA binding through either intercalation or external stacking.

With this in mind, we started considering the possibility of using platinum(II) and gold(III) complexes of the TPymT-α ligand for medicinal applications (Fig 1). TPymT-α shows peculiar and unique coordination chemistry properties: this ligand can in principle coordinate up to three metal ions at identical sites through a N3 donor set. However, only a limited number of studies employing this ligand have appeared so far owing to its generally poor solubility in common solvents and to the facile hydrolysis of the central triazine fragment [11].

In principle, the TPymT-α ligand is expected to give polynuclear Pt(II) and Au(III) complexes, each featuring a wide positively charged planar surface with aromatic character. These structural characteristics are known to favour binding toward nucleic acid structures, both in double helix and in G-quadruplex (G4) folding. Our efforts were first directed to the synthesis of the corresponding Pt complexes, and we succeeded in obtaining the $[Pt_3(TpymT)Cl_3]^{3+}$ species bearing three platinum cations coordinated by the N3 donor cavities and a chloride ligand as the fourth ligand, with three hydroxide anions as counterions [12].

However, solution studies revealed the occurrence of a non-intercalative interaction toward calf thymus DNA in the double helix B form, with a preferential external/groove binding [12]. As this behavior can be the likely result of a poor match between the wide triplatinum complex and the intercalative binding site of the DNA B-form, we decided to check the binding ability of different TpymT-α metal complexes toward G4.

Accordingly, we have carried out the reaction of the TpymT-α ligand with $HAuCl_4$ and characterised the resulting products (Figure 1). Afterwards, CD-melting experiments and crystallization screening were carried out to characterize the interaction of the obtained gold compounds with a 24-mer human telomeric DNA in quadruplex folding. One X-ray data set was good enough to solve the crystal structure of the human Tel24 G-quadruplex (Tel24 = $TAG_3(T_2AG_3)_3T$) in complex with the mononuclear $[(TpymT\text{-}\alpha)AuCl]^{2+}$ species, but refinement was difficult owing to the non-unique positioning of the complex on the guanine tetrad.

This kind of issue has been previously reported for several G4/ligand X-ray and NMR structures [13], and appears particularly important for metal complexes in square-planar or linear coordination geometries [14-16]. In order to better resolve this disorder issue and obtain a more certain and clear picture of the overall binding site for $[(TpymT\text{-}\alpha)AuCl]^{2+}$, we decided to test the reliability of the quantum refinement method. In quantum refinement, the empirical potential, which is employed in most macromolecular refinement to enhance the experimental data and ensure that reasonable bond lengths, angles and torsions are obtained, is replaced by more accurate quantum mechanical (QM) calculations [17]. This approach has been successfully applied to decide the protonation state of protein ligands, the oxidation state of metal ions and to decide the nature of bound ligands in protein structures. It is especially useful for metal sites, because they are hard to describe with empirical methods [17f]. It is also useful for sites with multiple conformations, for which it is hard to discern the various conformations in the poorly defined electron density [17c].

In the present study, an innovative approach based on a joint molecular mechanical (MM)/quantum mechanical (QM) calculation was used. The quantum-refinement software was modified and extended to sites with four conformations. Overall, the used method allowed to improve the crystallographic refinement for the adduct formed by Tel24 with $[(TpymT\text{-}\alpha)AuCl]^{2+}$, where the metal complex in the binding site is spread over four symmetry non-equivalent positions.

2. Experimental

2.1 Materials

The human telomeric DNA sequence $d[TAG_3(T_2AG_3)_3T]$ (Tel24) was purchased from Jena Bioscience as lyophilized material. Analytical grade reagents and ultra-pure water obtained through a Millipore S.A.670120 Mosheim apparatus were employed.

2.2 Synthesis

In a 50 mL flask, 5 mL of EtOH, 88 mg (0.28 mmol) of TpymT-α ligand and 1.7 mL of an aqueous solution of $HAuCl_4$ (339.8 mg/mL) were added. Subsequently, 82 mg of $NaHCO_3$ were added and the resulting mixture was stirred at 55 °C. After 2 h, the suspension was dried under reduced pressure and the remaining solid was suspended in 1.5 mL of H_2O. The suspension was filtered on a sintered glass funnel and the collected yellow solid was washed with water, diethyl ether and dried at reduced pressure. After desiccation, 188 mg of product (**I**) were collected.

2.3 DNA melting experiments

A UV-2450 SHIMADZU double-beam UV-vis spectrophotometer (Kyoto, Japan) was used for melting experiments. The instrument has a jacketed cell holder providing temperature control within ±0.1 °C. To avoid signal saturation, all spectra were recorded using 500 µL quartz cuvettes with an optical path of 2 mm. The thermal denaturation curves of Tel-24 G-quadruplex (G4) samples containing the investigated product (I) or the TPymT-α ligand, in a 1:3 molar ratio, were measured at increasing temperatures ranging from 25 °C to 65 °C following the absorbance changes at 290 nm. All the experiments were performed in 0.1 M ammonium acetate solution, pH 7.0. The percentage of absorbance change was plotted against temperature and defined as follows:

$$\%A \text{ change} = 100 \times (A(T) - A°)/(A\infty \times A°)$$

where A(T) is the absorbance read at each temperature T (°C), A° is the absorbance corresponding to the initial plateau and A∞ is the absorbance of the final plateau. In this way, a sigmoidal curve could be obtained. The melting temperature was calculated as the maximum of the first derivative of the sigmoidal curve.

2.4 Computationally enhanced X-ray diffraction analysis

Product (I) was dissolved in DMSO to a total 10 mM concentration, while the Tel24 sequence was dissolved in 20 mM potassium cacodylate pH 6.5 and 50 mM KCl up to a concentration 1 mM, and annealed to allow G-quadruplex formation by heating to 90 °C for 15 min and then slowly cooling to RT overnight. The stock DMSO solution was added to the DNA annealed solution in 1:1 product (I):DNA molar ratio and the resulting solution was incubated at 25 °C for 20 min. Crystallization trials were set up by mixing 1 µL DNA–drug complex solution with 1 µL crystallization solution. Crystals of $[(TpymT\text{-}\alpha)AuCl]^{2+}$ / Tel24 suitable for SC-XD analysis were obtained at 296 K using the sitting drop vapor diffusion method from a solution containing 20% v/v isopropanol, 50 mM potassium cacodylate pH 6.5, 50 mM Li_2SO_4, 50 mM $MgSO_4$, on the basis of a reported screening [18]. Drops were equilibrated against the same solution (100 µL).

The $[(TpymT\text{-}\alpha)AuCl]^{2+}$ / Tel24 complex crystallizes in the monoclinic system, space group C2 (a = 36.78 Å, b = 71.53 Å, c = 26.24 Å, β = 92.42°). Data collection was performed using synchrotron light (λ = 0.87313 Å, ID23-1 Beamline, ESRF Grenoble). Data were collected at 100 K, using the crystallization solution added with glycerol up to 30% v/v as cryoprotectant. Data were integrated and scaled using the program XDS [19]. The structure was solved by the Molecular Replacement technique using the program MOLREP [20] and the coordinates of the Tel24 G-quadruplex structure PDB-6H5R [16], without all the heteroatoms, as a search model. The model was refined with the program Refmac5 [21] from the CCP4 program suite [22]. Manual rebuilding of the model was performed using the program Coot [23]. For the T24 residue, only the phosphate group was clearly visible in the electron density map, thus only those coordinates were refined.

The model obtained at this step of refinement consisted of the overall DNA coordinates, potassium ions, and a gold ion, spread over four sites (0.25 occupancy factor each).

Restrained docking calculations were carried out to obtain a preliminary positioning of the overall ligand spread over the four sites. The model was prepared using the Protein Preparation Wizard tool implemented in the Schrödinger suite [24]. The energy minimization protocol with a root mean square deviation (RMSD) value of 0.30 Å was applied using the OPLS3e force field. The Au ion complex was submitted to quantum mechanics geometry optimization (B3LYP/LACVP**+) and ESP charge calculation with Jaguar [24a]. Standard precision (SP) docking experiments were carried out using the software Glide [24b] and the QM charges. Four grids were prepared, each centred on one of the Au^{3+} ions. A positional constraint for the ligand was set on the Au^{3+} ion to be docked within 0.5 Å of the metal ion position detected experimentally. The highest docking score criterion was used to select a single pose per gold ion out of a maximum of five docking outcomes.

The docked structure was then used as the starting structure for quantum refinement [17a,b]. Quantum refinement is standard crystallographic refinement in which the empirical restraints (used to ensure that the final structure gives reasonable bond lengths and angles) are replaced by more accurate quantum mechanical (QM) calculations for a small, but interesting part of the structure. This approach was recently extended to allow for multiple conformations in the QM system [17c]. In the present study, it was further extended to four conformations in the QM system, by simply performing four separate QM calculations for each conformation. Further details of the implementation are given in the ESI. The calculations were performed with the ComQum-X software [17a]. which is a combination of Turbomole [25] and the crystallography and NMR system (CNS), version 1.3 [26].

The full Tel24 G-quadruplex was used in all calculations, including all crystal-water molecules. For the DNA, we used the standard CNS force field (dna-rna_rep.param, water_rep.param and ion.param). The wA factor (determining the relative weight between the crystallographic data and the empirical potential, cf. Eqn. 2 in the ESI) was the default value suggested by CNS, 4.153. The wMM weight was set to 1/3 as in all our previous studies [17a,c]. For the crystallographic target function, we used the standard maximum-likelihood function using amplitudes (mlf) in CNS [27].

The QM system involved four copies of the (TpymT-α)AuCl complex (we tested also OH^- instead of Cl^- coordinated to the Au ion, but the fit to the crystallographic data was worse). Calculations were performed for the triplet and (closed-shell) singlet states, but the singlet was found to be lowest in energy by ~60 kJ/mol and will only be discussed in the following. The QM calculations were performed at the TPSS/def2-SV(P) level of theory (including a 60-electron relativistic effective core potential for Au) [28]. The calculations were sped up by expanding the Coulomb interactions in an auxiliary basis set, the resolution-of-identity (RI) approximation [29]. Empirical dispersion corrections were included with the DFT-D3 approach [30] and Becke–Johnson damping [31].

Finally, a few refinement cycles were performed with the software Refmac5 [21] in order to obtain final refinement statistics. These values as well data collection information are reported in Table S2, supporting information.† Final coordinates and structure factors have been deposited with the Protein Data Bank (PDB accession number 7QVQ).

3. Results and discussion

3.1 Synthesis of gold(III) complexes of the TpymT-α ligand

By analogy with the previously synthesised $[Pt_3(TpymT)Cl_3]^{3+}$ complex we aimed to prepare the corresponding trinuclear complex where three gold atoms are coordinated by the TpymT-α ligand. Thus, the TpymT-α ligand was reacted with an excess of tetrachloroauric acid and a solid product obtained as described in the experimental section. The obtained product (I) was subsequently characterized by a variety of biophysical methods including ^{1}H NMR, IR spectroscopy, and elemental analysis. Based on these analytical determinations, we realized that the obtained product is indeed a mixture of two main species, i.e. $[Au_2L]$ and [AuL] (charges and coordinated anions omitted here and in the following). More precisely, the CHN analysis suggested that the two species $[(TpymT\text{-}\alpha)AuCl]Cl_2$ and $[(TpymT\text{-}\alpha)Au_2Cl_2]Cl_4$ (Table S1 – supporting material) are present in nearly equal amounts.

Unfortunately, all attempts to separate the two species $[(TpymT\text{-}\alpha)AuCl]Cl_2$ and $[(TpymT\text{-}\alpha)Au_2Cl_2]Cl_4$ failed. For this reason, the whole mixture was used as such for the subsequent studies. From the inspection of the IR spectrum of (I) (see Figure S1 in supporting material), three main bands were detected at 358 cm^{-1}, 318 cm^{-1}, and 230 cm^{-1} attributable to the Au-Cl, N-Au-Cl and Au-N modes, respectively [32] providing additional evidence for the presence of chloride as the fourth ligand of the gold(III) center. Product (I) is poorly soluble in water, while manifesting a greater solubility in DMSO.

3.2 DNA melting experiments

Spurred by the aforementioned evidence and upon considering the ligand structure and the likely planar structure of the gold(III) complexes contained in the product (I), we started investigating the interaction of this product with the Tel24 G-quadruplex that is known to manifest a preference for planar compounds containing aromatic groups. DNA melting studies were first performed to demonstrate the occurrence of a sufficiently tight interaction in solution. Tel24 G-quadruplex and the product (I) or the TpymT-α ligand were thus reacted at room temperature in a molar ratio $C_{product\ (I)}/C_{G4} = C_{ligand}/C_{G4} = 3$. An excess of the reactive molecules with respect to the DNA structure was used both to ensure a sufficient amount of the possible formed adducts that could be observed by this analysis, and also to provide a suitable amount of the reacting molecule for all the possible biomolecule's binding sites. Results of the melting experiments are shown in Figure 2 and in Table S3. From inspection of these data, it emerges that product (I) is able to significantly modify the melting profile of the Tel24 G quadruplex. In detail, binding of (I) results in a small but clear destabilisation of the Tel24 G quadruplex by around 2 °C. We interpret this decrease of the melting temperature as the indication of the occurrence of a direct interaction between the Tel24 G quadruplex and product (I).

3.3 Computationally enhanced X-ray diffraction analysis

Crystals suitable for X-ray diffraction analysis were obtained upon incubation of the telomeric DNA sequence Tel24 with the product (I) under the crystallization conditions described in the Experimental section. The electron density map clearly shows monomolecular DNA G-quadruplexes arranged in columns growing along the c axis (Figure 3). The HT-quadruplexes are known to be highly polymorphic, depending on the experimental conditions adopted. In the solid-state, they usually assume the all parallel conformation (Figure 1 top), characterized by propeller loops, three stacked G-tetrads at 3.4 Å inter-planar distance, and potassium ions in the internal channel (2.6–3.1 Å apart from the guanine O6 atoms). Notably, the all parallel structure has been reported, both in

solution and in the solid-state, also for other quadruplex forming sequences, such as the TERRA-RNA, the c-Myc and the c-kit DNA [1b].

In our structure, pairs of G4 units, symmetry-related by two-fold rotation axis, stack on one another forming dimers stabilized by the presence of a potassium ion at the interface between 5'-end G-tetrads in each couple of adjacent quadruplexes.

Similar G4 couples, stabilized by potassium [8,14,33] or strontium ions [16], have previously been reported. The G4 dimers expose their 3'-end guanine tetrads, which constitute the ligand binding site. Actually, the 3′-end G-tetrads from symmetry-related dimers repeating along the c axis, lie about 10 Å apart from one another. In the resulting cavity, eight prominent peaks were evident in the electron density map, which can be split in two groups and overall assigned to two symmetry-related gold ions, each spread over four almost coplanar positions. A similar disordered binding mode was previously found for the bis carbene gold(I) complex [Au(1-butyl-3-methyl-2-ylidene)$_2$]$^+$ in adduct with a propeller telomeric quadruplex [16], where two symmetry-related disordered gold complexes, each spread over four approximately coplanar positions, were suggested to be present in the binding site.

Since the product (I) is an almost equimolar mixture of mononuclear [(TpymT-)AuCl]Cl2 and binuclear [(TpymT-α)Au$_2$Cl$_2$]Cl$_4$, we have to take into account the possibility that the mononuclear complex alone, the binuclear one or a combination of the two could have been cocrystallized with the DNA. An investigation of the Cambridge Structural Database [34] revealed that in the bi- and trinuclear complexes of TpymT-α, containing second- or third-row transition metal ions, intramolecular intermetallic distances are 6.5–7 Å. This data led us to eliminate the hypothesis that only the binuclear complex could have been cocrystallized with DNA. In fact, among the three longest inter-metallic distances between the four coplanar gold ions in the crystal structure of the binding site (about 5, 6 and 7 Å), only one of them is compatible with the expected intramolecular intra-gold distance of a binuclear complex. On the other hand, the hypothesis of a mixture of [(TpymT-α)AuCl]/DNA and [(TpymT-α)Au$_2$Cl$_2$]/DNA in 2:1 molar ratio was discarded, as almost the same amount of electrons was associated with each of the four peaks, leading to equally populated gold positions. Thus, two symmetry-related mononuclear gold complexes, each one spread over four approximately coplanar positions, seem to fit the crystallographic data best.

Unfortunately, the residual electron density did not allow a clear localization of the lighter atoms (C and N). Therefore, we first obtained tentative locations of the four metal complexes in the asymmetric unit on the 3'-end tetrad by restrained molecular docking (see section 2.4 for details). Then, these positions were refined, with fractional occupation factors (0.25), against the observed structure factors by the ComQumX-4QM method [17]. In this approach, the QM calculations ensure that the structures of the (TpymT-α)AuCl complexes are chemically reasonable, but at the same time they are fitted to the experimental data. Therefore, it provides structures that are an optimal compromise between the crystallographic raw data and the QM calculations. The resulting structures are shown in Figure 4. Each [(TpymT-α)AuCl] molecule is found at π–π stacking distance from the nearest 3'-end G-tetrad (3.3 Å), and at even closer interplanar distance (about 3.1 Å) from the symmetry-related [(TpymT-α)AuCl] molecules (Figure 3).

As shown in Figure 4, the TpymT- α moieties match the guanine tetrad well. In [(TpymT-α)AuCl]- C (Figure 4b), [(TpymT-α)AuCl]-E (Figure 4d) and [(TpymT-α)AuCl]-F (Figure 4e), the triazine ring is placed over the G4 central channel, and all the three pyrimidine rings give π-stacking interaction with an equivalent number of guanine residues. The

gold(III) metal ion is placed in close proximity (3.4–3.7 Å) to the carbonyl oxygen and the N7 nitrogen of G5 and G11 ([(TpymT- α)AuCl]-C and [(TpymT-α)AuCl]-E, respectively), or to the O6 and N7, and the N1 and N2 heteroatoms of G23 and G17, respectively ([(TpymT-α)AuCl]-F). The position of the fourth complex ([(TpymT-α)AuCl]-D, Figure 4c) shows distinct binding features, with the gold center placed above the potassium channel. The π-stacking interaction involves mainly a pyrimidine group and the triazine unit of the ligand, and only two guanines in the 3'-end tetrad (G5 and G11). The non-coordinated pyrimidine is placed above the G11 ribose, giving a slight loss of planarity of the overall TpymT-α moiety. Still, the metal complexes in the four conformations have essentially the same intrinsic QM energy (within 4 kJ/mol; [(TpymT-α)AuCl]-F lowest, [(TpymT-α)AuCl]-C highest), and they are very little strained compared to the optimum vacuum structure, by only 3–6 kJ/mol. This shows that the structures are reasonable and fit the crystallographic data well. No water molecules were found in the binding site at contact distance with the coordinated chloride or the free pyrimidine nitrogens.

Thus, despite the disorder affecting the binding site, in our opinion this crystal structure evidences the binding preferences of Au(III)-TpymT- α toward the telomeric G-quadruplexes, as in three out of four observed ligand positions, the metallodrug gives almost the same kind of interactions.

Actually, the good conformational match between the three pyrimidines and the guanines residues seems to be the main driving force for the binding of the Tpymt ligand, and the resulting π–π stacking provides an important contribution to the stability of the adduct. Moreover, it is likely that in [(TpymT-α)AuCl]-C, [(TpymT-α)AuCl]-E and [(TpymT-α)AuCl]-F (Figure 4b,d,e), triazine ring does not only play the role of linker group, but it also contributes itself to the overall binding.

In fact, triazine, being an electron-poor heteroaromatic ring, is known to possess an inverted molecular quadrupole moment compared to benzene and other electron-rich aromatic groups. The inversion of the quadrupole moment is connected to the accumulation of positive charge towards the ring centre, while the periphery of the ring becomes negative. This phenomenon turns the electron-poor aromatic system into a π-acid, known to be able to give attractive interactions with anions and lone-pair bearing atoms [35]. Thus, when placed over the G4 central channel, triazine likely exerts an analogous charge–charge neutralizing action, thereby contributing to the overall stabilization of the system.

It is to be underlined that, the negatively charged central channel determined by the guanine carbonyl oxygens, is a G-quadruplex essential element, present independently from the polymorphic folding adopted. This structural feature, which additionally requires the presence of neutralizing alkali cations, has been used in the design of most of the metal-based quadruplex binders up to now developed. In fact, the XRD and NMR structures obtained point out the tendency of these binders to stack with the electropositive metal positioned at the center of a G-quartet, in a way that the metal center can be considered to play the same role as the alkali metal cation in an hypothetic additional guanine quartet. . From this point of view, the central π-acidic triazine of TpymT-α represents a new possible building block for the rational design of G-quadruplex binders. In addition, interesting comparisons can be made made with the gold(I) complexes, $[Au(1\text{-butyl-3-methyl-2-ylidene})_2]^+$ and $[Au(9\text{-methylcaffein-8-ylidene})_2]^+$, complexed with telomeric DNA quadruplex, whose crystal structures have been previously reported [14,16]. In these structures, the gold(I) ions are never found at the central channel, but they always interact with guanines and are placed at about 3.5 Å from N1 nitrogens. Thus, despite the high oxidation state of gold in [(TpymT-α)AuCl], which should favour the metal ion being at the central channel, the bulky TpymT-α

structure disfavours this placement, and the binding preferences of this metallodrug are due to a combined effect of pyrimidine stacking, metal–guanine interactions and charge–charge neutralizing actions of triazine's inverted quadrupole moment.

Conclusions

The reaction of the ligand 2,4,6-tris(2-pyrimidyl)-1,3,5-triazine (TpymT-α, L) with an excess of tetrachloroauric acid yields a product (I) that turned out to be a nearly equimolar mixture of the mono and bis gold(III) complexes [AuL] and [Au2L]. Both these species bear tetracoordinate square planar gold(III) centers with chloride as the fourth ligand. Melting experiments provided evidence for the formation of an adduct between product (I) and human telomeric DNA Tel24 G-quadruplex. The reported crystal structure documents the occurrence of a fishing-like crystallization process, in which only the [AuL] species is selectively bound to the telomeric G-quadruplex.

Structural results, aided by MM restrained docking, were obtained applying crystallographic refinement enhanced with QM calculation. The described method has been specifically developed to enable us to resolve issues with poor electron density due to the spreading of the mononuclear complex [(TpymT-α)AuCl] over four equally populated positions, stacked at the 3'-end G-tetrad of the telomeric quadruplex. Analysis of the obtained crystal structure revealed that the binding preferences of this metallodrug arise from a combined effect of pyrimidine stacking, metal–guanine interactions and charge–charge neutralizing action of triazine's inverted quadrupole moment.

Acknowledgements

The authors gratefully acknowledge Prof. Roberto Bini (LENS, University of Florence) for acquisition of the IR spectrum.

Fundings

This work was supported by the Fondazione Cassa di Risparmio di Firenze (ERC, project number 23942.2019); the Swedish research council (grants numbers 2018-05003 and 2020-06176); the eSSENCE e-science collaboration; the Associazione Italiana per la Ricerca sul Cancro (AIRC, grant number 23852); the University of Pisa (PRA 2020_39); the Beneficentia Stiftung (Vaduz, BEN2020/34). The computations were performed on computer resources provided by the Swedish National Infrastructure for Computing (SNIC) at Lunarc at Lund University and HPC2N at Umeå University, partially funded by the Swedish Research Council (grant 2018-05973).

Author contributions

Damiano Cirri: Investigation, Formal analysis. *Carla Bazzicalupi*: Conceptualization, Formal analysis, Funding acquisition; Writing – Original draft and Review and Editing, Visualization, Validation. Project administration. *Ulf Ryde*: Formal analysis, Writing – Original draft and Review and Editing, Visualization, Funding acquisition. *Justin Bergmann*: Investigation, Formal analysis. *Francesca Binacchi:* Investigation, Formal analysis. *Alessio Nocentini*: Investigation, Formal analysis. *Alessandro Pratesi*: Investigation, Formal analysis, Funding acquisition. *Paola Gratteri*: Conceptualization,

Formal analysis, Funding acquisition; Writing – Original draft and Review and Editing, Visualization, Validation. Project administration. *Luigi Messori*: Formal analysis, Investigation, Writing – Original draft and Review and Editing, Visualization.

References

[1]a) D. Rhodes, H. J. Lipps, G-quadruplexes and their regulatory roles in biology, Nucleic Acids Res. 43 (2015) 8627–8637. https://doi.org/10.1093/nar/gkv862; b) H. L. Lightfoot, T. Hagen, N. J. Tatum, J. Hall, The diverse structural landscape of quadruplexes, FEBS Letters 593 (2019) 2083– 2102. https://doi.org/10.1002/1873-3468.13547.

[2] a) E. Ruggiero, S. N. Richter, G-quadruplexes and G-quadruplex ligands: targets and tools in antiviral therapy, Nucleic Acids Res. 46 (2018) 3270 – 3283. https://doi.org/10.1093/nar/gky187; b) F. Dumetz, C. J. Merrick, Parasitic protozoa: unusual roles for G-quadruplexes in early-diverging eukaryotes Molecules 24 (2019) 1339–1350. https://doi.org/10.3390/molecules24071339

[3] A.K. Todd, M. Johnston, S. Neidle, Highly prevalent putative quadruplex sequence motifs in human DNA. Nucleic Acids Res. 33 (2005), 2901–2907. https://doi.org/10.1093/nar/gki553.

[4] E. Henderson, C.C. Hardin, S.K. Walk, I.Jr Tinoco, E.H. Blackburn, Telomeric DNA

oligonucleotides form novel intramolecular structures containing guanine-guanine base pairs, Cell., 51 (1987) 899–908. https://doi.org/10.1016/0092-8674(87)90577-0

[5] Q. Cao, Y. Li, E. Freisinger, P. Z. Qin, R. K. O. Siegel, Z.-W. Mao, G-quadruplex DNA targeted metal complexes acting as potential anticancer drugs, Inorg. Chem. Front. 4, (2017), 10–32. https://doi.org/10.1039/C6QI00300A

[6] A. R. Duarte, E. Cadoni, A. S. Ressurreição, R. Moreira, A. Paulo, Design of Modular G-quadruplex Ligands, ChemMedChem 2018, 13, 869–893. https://doi.org/10.1002/cmdc.201700747.

[7] E. Palma, J. Carvalho, C. Cruz, A. Paulo, Metal-Based G-Quadruplex Binders for Cancer Theranostics, Pharmaceuticals 2021, 14, 605. https://doi.org/10.3390/ph14070605

[8] H. M. Berman, J. Westbrook, Z. Feng, G. Gilliland, T. N. Bhat, H. Weissig, I. N. Shindyalov, P. E. Bourne, The Protein Data Bank, Nucleic Acids Res., 28 (2000) 235-42. https://doi.org/10.1093/nar/28.1.235.

[9] L. Massai, D. Cirri, E. Michelucci, G. Bartoli, A. Guerri, M.A. Cinellu, F. Cocco, C. Gabbiani, L.Messori, Organogold(III) compounds as experimental anticancer agents: chemical and biological profiles, Biometals 29 (2016) 863–872. https://doi.org/10.1007/s10534-016-9957-x.

[10] B. D. Glisic, M. I. Djuran, Gold complexes as antimicrobial agents: an overview of different biological activities in relation to the oxidation state of the gold ion and the ligand structure, Dalton Trans., 43 (2014) 5950-5969. https://doi.org/10.1039/c4dt00022f

[11] D.A. Safin, J. M. Frosta, M. Murugesu, The renaissance of 2,4,6-tris(2-pyrimidyl)-1,3,5-triazine (TPymT) coordination chemistry, Dalton Trans. 44 (2015) 20287-20294. https://doi.org/10.1039/c5dt03435c

[12] T. Marzo, D. Cirri, L. Ciofi, C. Gabbiani, A. Feis, N. Di Pasquale, M. Stefanini, T. Biver, L. Messori, Synthesis, characterization and DNA interactions of [Pt3(TpymT)Cl3], the trinuclear platinum(II) complex of the TpymT ligand, J.Inorg. Biochem. 183 (2018) 101–106. https://doi.org/10.1016/j.jinorgbio.2018.03.009.

[13] J. Dickerhoff, N. Brundridge, S.A. McLuckey, D. Yang, Berberine Molecular Recognition of the Parallel MYC G-Quadruplex in Solution J. Med. Chem. 64 (2021) 16205-16212. https://doi.org/10.1021/acs.jmedchem.1c01508

[14] N.H. Campbell, N.H. Abd Karim, G.N. Parkinson, M. Gunaratnam, V. Petrucci, A.K. Todd, R. Vilar, S. Neidle, Molecular Basis of Structure–Activity Relationships between Salphen Metal Complexes and Human Telomeric DNA Quadruplexes, J. Med. Chem. 55 (2012) 209−222. https://doi.org/10.1021/jm201140v.

[15] C. Bazzicalupi, M. Ferraroni, F. Papi, L. Massai, B. Bertrand, L. Messori, P. Gratteri, A. Casini, Determinants for Tight and Selective Binding of a Medicinal Dicarbene Gold(I) Complex to a Telomeric DNA G-Quadruplex: a Joint ESI MS and XRD Investigation, Angew. Chem. Int. Ed. 55 (2016) 4256-4259. https://doi.org/10.1002/anie.201511999.

[16] F. Guarra, T. Marzo, M. Ferraroni, F. Papi, C. Bazzicalupi, P. Gratteri, G. Pescitelli, L. Messori, T. Biver, C. Gabbiani, C. Dalton Trans., 47 (2018) 16132-16138. https://doi.org/10.1039/C8DT03607A.

[17] a) U. Ryde, L. Olsen, K. Nilsson, Quantum chemical geometry optimisations in proteins using crystallographic raw data, J. Comp. Chem., 23 (2002) 1058-1070. https://doi.org/10.1002/jcc.10093; b) J. Bergmann, E. Oksanen, U. Ryde, Combining crystallography with quantum mechanics, Curr. Opin. Struct. Biol., 72 (2021) 18-26. https://doi.org/10.1016/j.sbi.2021.07.002; c) L. Cao, U. Ryde, Quantum refinement with multiple conformations: Application to the P-cluster in nitrogenaseActa Crystal. D, 76 (2020) 1145-1156. https://doi.org/10.1107/S2059798320012917; d) L. Cao, O. Caldararu, U. Ryde, Does the crystal structure of vanadium nitrogenase contain a reaction intermediate? Evidence from quantum refinement, J. Biol. Inorg. Chem., 25 (2020) 847-861. https://doi.org/10.1007/s00775-020-01813-z; e) L. Cao, O. Caldararu, A. C. Rosenzweig, U. Ryde, Quantum Refinement Does Not Support Dinuclear Copper Sites in Crystal Structures of Particulate Methane Monooxygenase, Angew. Chem., Int. Ed., 57 (2018), 162–166. https://doi.org/10.1002/anie.201708977; f) L. Hu, U. Ryde, Comparison of methods to obtain force-field parameters for metal sites, J. Chem. Theory Comput. (2011), 7, 2452-2463. https://doi.org/10.1021/ct100725a

[18] N. H. Campbell, G. N. Parkinson, Crystallographic studies of quadruplex nucleic acids. Methods 43 (2007) 252–263. https://doi.org/10.1016/j.ymeth.2007.08.005.

[19] W. Kabsch, XDS, Acta Cryst., D66 (2010) 125–132. https://doi.org/10.1107/S0907444909047337.

[20] A. Vagin, A. Teplyakov, MOLREP: an Automated Program for Molecular Replacement, J. Appl. Cryst. 30, (1997) 1022–1025. https://doi.org/10.1107/S0021889897006766.

[21] G.N. Murshudov, A.A. Vagin, E.J. Dodson, Refinement of macromolecular structures by the maximum-likelihood method, Acta Crystallogr. D 53 (1997) 240-255. https://doi.org/10.1107/S0907444996012255.

[22] M.D. Winn, C.C. Ballard, K.D. Cowtan, E.J. Dodson, P. Emsley, P.R. Evans, R.M. Keegan, E.B. Krissinel, A.G.W. Leslie, A. McCoy, S.J. McNicholas, G.N. Murshudov, N.S. Pannu, E.A. Potterton, H.R. Powell, R.J. Read, A. Vagin, K.S. Wilson, Overview of the

CCP4 suite and current developments, Acta Crystallogr D 67 (2011) 235-242. https://doi.org/10.1107/S0907444910045749.

[23] P. Emsley, B. Lohkamp, W.G. Scott, K. Cowtan, Features and development of Coot, Acta Crystallogr 66D (2010) 486-501. Doi: https://doi.org/10.1107/S0907444910007493.

[24] Schrödinger Suite Release 2019-4, Schrödinger, LLC, New York, NY, 2019. A) Jaguar, v.10.3; b) Glide, v.8.2.

[25] F. Furche, R. Ahlrichs, C. Hättig, W. Klopper, M. Sierka, F. Weigendet, Turbomole, WIREs Comput Mol Sci. 4 (2014) 91–100. https://doi.org/10.1002/wcms.1162

[26] A.T. Brunger, P.D. Adams, G.M. Clore, W.L. DeLano, P. Gros, R.W. Grosse-Kunstleve, J.S. Jiang, J. Kuszewski, M. Nilges, N.S. Pannu, R.J. Read, L.M. Rice, T. Simonson, G. L. Warren, Crystallography & NMR system: A new software suite for macromolecular structure determination, Acta Crystallogr. D 54 (1998):905–921. https://doi.org/10.1107/s0907444998003254; b) A.T. Brunger, Version 1.2 of the Crystallography and NMR system, Nat Protoc 2 (2007) 2728–33. https://doi.org/10.1038/nprot.2007.406.

[27] a) N.S. Pannu, R.J. Read, Improved Structure Refinement Through Maximum Likelihood, Acta Crystallogr Sect A Found Crystallogr A52 (1996) 659–668. https://doi.org/10.1107/S0108767396004370; b) P.D. Adams, N.S. Pannu, R.J. Read, A.T. Brünger, Cross-validated maximum likelihood enhances crystallographic simulated annealing refinement, Proc Natl Acad Sci U S A 94 (1997)5018–5023. https://doi.org/10.1073/pnas.94.10.5018.

[28] a) J. Tao, J.P. Perdew, V.N. Staroverov, G.E. Scuseria, Climbing the Density Functional Ladder: Nonempirical Meta–Generalized Gradient Approximation Designed for Molecules and Solids, Phys Rev Lett 91 (2003) 146401. https://doi.org/10.1103/PhysRevLett.91.146401; b) A. Schäfer, H. Horn, R. Ahlrichs, Fully optimized contracted Gaussian basis sets for atoms Li to Kr, J Chem Phys 97 (1992) 2571–2577. https://doi.org/10.1063/1.463096

[29] a) K. Eichkorn, O. Treutler, H. Öhm, M. Häser, R. Ahlrichs, Auxiliary basis sets to approximate Coulomb potentials, Chem Phys Lett 240 (1995) 283–289. https://doi.org/10.1016/0009-2614(95)00621-a; b) K. Eichkorn, F. Weigend, O. Treutler, R. Ahlrichs Auxiliary basis sets for main row atoms and transition metals and their use to approximate Coulomb potentials, Theor. Chem. Acc. 97 (1997) 119–124. https://doi.org/10.1007/s002140050244.

[30] S. Grimme, J. Antony, S. Ehrlich, H. Krieg, A consistent and accurate ab initio parametrization of density functional dispersion correction (DFT-D) for the 94 elements H-Pu, J. Chem. Phys. 132 (2010) 154104 (19 pages). https://doi.org/10.1063/1.3382344

[31] S. Grimme, S. Ehrlich, L. Goerigk, Effect of the damping function in dispersion corrected density functional theory, J. Comput. Chem. 32 (2011) 1456–1465. https://doi.org/10.1002/jcc.21759.

[32] a) E.A. Allen, W. Wilkinson, Spectrochimica Acta, 28A (1972), 2257- 2262. https://doi.org/10.1016/0584-8539(72)80200-9; b) D.R. Williamson, M.C. Baird, Gold-halogen stretching frequencies, J. Inorg. Nucl. Chem. 34 (1972) 3393-3400. https://doi.org/10.1016/0022-1902(72)80233-1.

[33] PDB codes: 1KF1, 2HRI, 3CCO, 3QSC, 3QSF, 3UYH, 4DA3,4DAQ, 3SC8, 3TSE, 4FXM, 4G0F, 5DWX, 5DWW

[34] F.H. Allen, The Cambridge Structural Database: a quarter of a million crystal structures and rising, Acta Cryst. B58 (2002) 380—388. https://doi.org/10.1107/S0108768102003890. The CSD version used in this work was updated in 2021.

[35] M. Savastano, C. García-Gallarín, M.D. López de la Torre, C. Bazzicalupi, A. Bianchi, M. Melguizo, Anion Complexes with Tetrazine-Based Ligands: Formation of Strong Anion−π Interactions in Solution and in the Solid State, Coord. Chem. Rev. 397 (2019) 112–137. https://doi.org/10.1021/acs.inorgchem.6b01138.

Captions to illustrations

Figure 1. Top: square planar arrangement of four guanines stabilized by Hoogsteen hydrogen bonds and by the central metal cation (G-tetrad or G-quartet - left) and all parallel G4 folding (right). Bottom: Chemical structure of the gold(III) complexes obtained by reaction of the TpymT-α ligand. Both complexes coordinate exogenous chloride ligands.

Figure 2. Melting plot of G4 alone (■) (CG4 = 9.90×10-6 M) and G4 with product (I) (●), or TpymT- α ligand (▲), Cproduct (I)/CG4 = Cligand/CG4 = 3, Nh4OAc 0.1 M, pH = 7.0.

Figure 3. Column of stacked G-quadruplexes in the crystal packing of the Tel24/[(TpymT-α)AuCl] crystal structure. K+ ions are shown as purple spheres (inset: [(TpymT-α)AuCl]/G-quartet π-stacking distances in Å)

Figure 4. a) Skeleton of the [(TpymT-α)AuCl] complex, spread over four positions. OMIT electron density map contoured at 2σ level; b-e) Details of each single position of the [(TpymT-α)AuCl] gold-complex stacked on the 3'-end G-tetrad. Color code for the carbon atoms of the four approximately coplanar disordered [(TpymT-α)AuCl] molecules stacked on the 3'-end G-tetrads defining the binding site: [(TpymT-α)AuCl]-C (by element), [(TpymT-α)AuCl]-D (green), [(TpymT-α)AuCl]-E (orange red), [(TpymT-α)AuCl]-F (orange), symmetry related [(TpymT- α)AuCl] molecules (black).

Figure 1

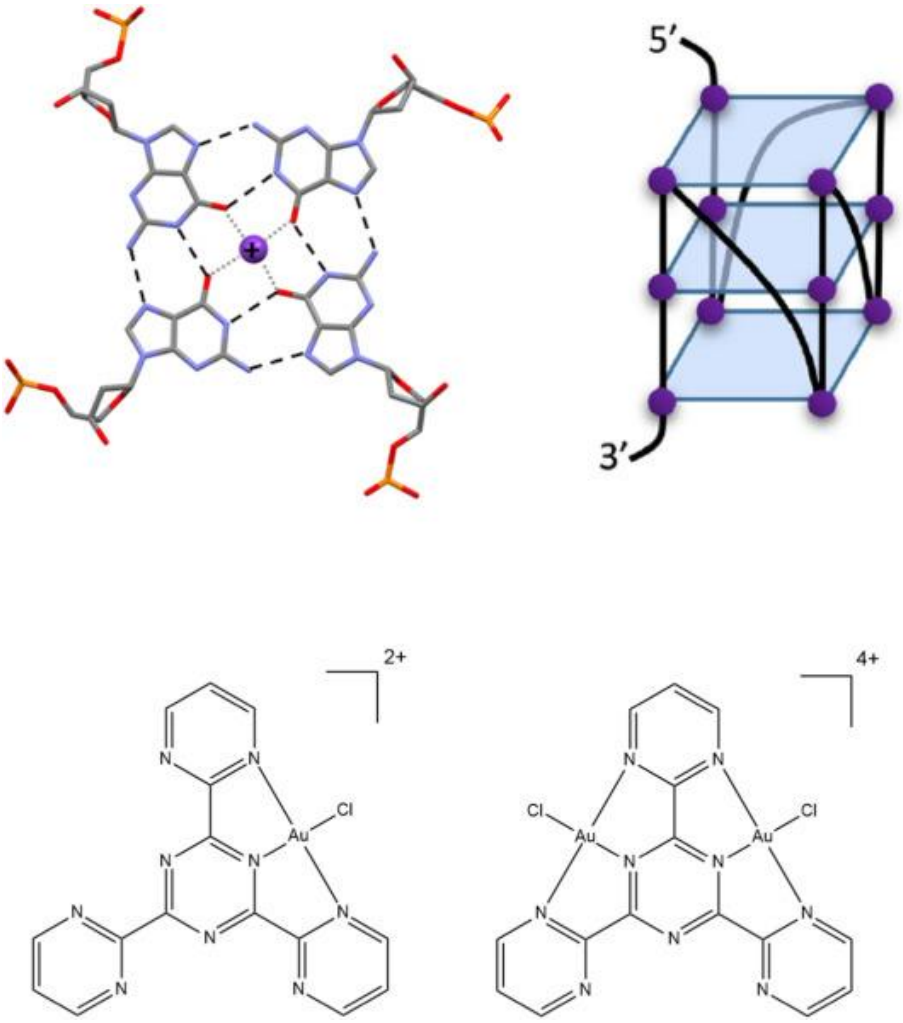

Figure 2.

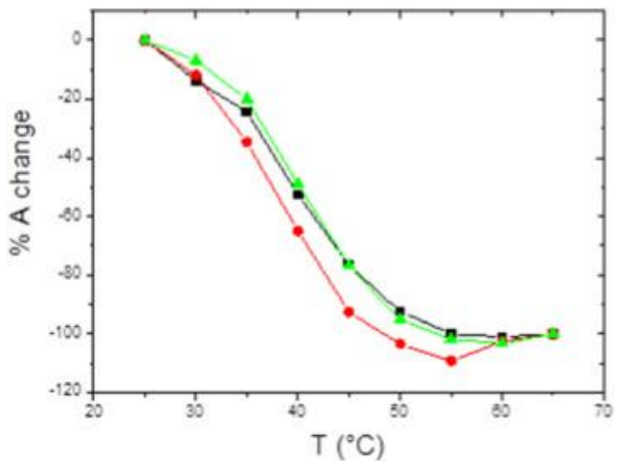

Figure 3.

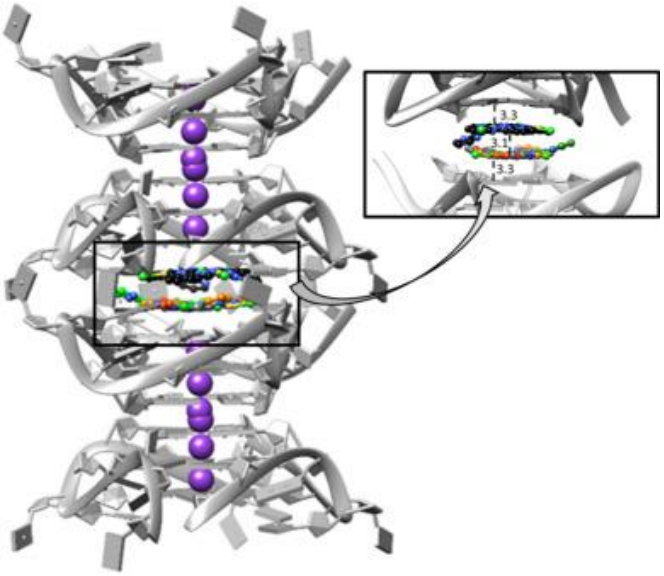

Figure 4.